

NE2001. I. A NEW MODEL FOR THE GALACTIC DISTRIBUTION
OF FREE ELECTRONS AND ITS FLUCTUATIONS

J. M. CORDES

Astronomy Department and NAIC, Cornell University, Ithaca, NY 14853
cordes@spacenet.tn.cornell.edu

T. JOSEPH W. LAZIO

Naval Research Lab, Code 7213, Washington, D.C. 20375-5351
Joseph.Lazio@nrl.navy.mil*Draft version October 23, 2018*

ABSTRACT

We present a new model for the Galactic distribution of free electrons. It (a) describes the distribution of the free electrons responsible for pulsar dispersion measures and thus can be used for estimating the distances to pulsars; (b) describes large-scale variations in the strength of fluctuations in electron density that underly interstellar scattering; (c) can be used to interpret interstellar scattering and scintillation observations of Galactic objects and of extragalactic objects, such as intrinsically compact AGNs and Gamma-ray burst afterglows; and (d) serves as a preliminary, smooth spatial model of the warm ionized component of the interstellar gas. This work builds upon and supersedes the Taylor & Cordes (1993) model by exploiting new observations and methods, including (1) a near doubling in the number of lines of sight with dispersion measure or scattering measurements; (2) a substantial increase in the number and quality of independent distance measurements or constraints; (3) improved constraints on the strength and distribution of scattering in the Galactic center; (4) improved constraints on the (Galactocentric) radial distribution of free electrons; (5) redefinition of the Galaxy’s spiral arms, including the influence of a local arm; (6) modeling of the local interstellar medium, including the local hot bubble identified in X-ray and Na I absorption measurements; and (7) an improved likelihood analysis for constraining the model parameters. For lines of sight directed out of the Galactic plane, the new model yields substantially larger values for pulsar dispersion measures, except for directions dominated by the local hot bubble. Unlike the TC93 model, the new model provides sufficient electrons to account for the dispersion measures of the vast majority of known, Galactic pulsars. The new model is described and exemplified using plots of astronomically useful quantities on Galactic-coordinate grids. Software available on the Internet is also described. Future observations and analysis techniques that will improve the Galactic model are outlined.

Subject headings: distance measurements, interstellar medium, electron density, pulsars

1. INTRODUCTION

Radio wave propagation measurements provide unique information about the magnetoionic component of the interstellar medium (ISM). Pulsars are important probes because they emit short duration radio pulses that are modified by intervening plasma and also because they are highly spatially coherent, allowing scattering processes to significantly perturb their radiation. Other compact sources, both Galactic and extragalactic, also serve as probes of the plasma.

In this first of a series of papers, we present a new model for the free electron density of the Galaxy. It is called “NE2001” because it incorporates data obtained or published through the end of 2001. A short history of such models prior to 1993 is given in Taylor & Cordes (1993, hereafter TC93). Our work builds upon and supersedes the TC93 model by exploiting new dispersion and scattering measurements and also by employing new techniques for modeling. Following Cordes et al. (1991) and TC93, we model fluctuations in electron density as well as the local mean density.

Since TC93 was written, significant developments

have taken place that increase the sample of relevant measurements and indicate shortcomings of the model. Most importantly, independent distance measurements are available on about 50% more objects. Some of these are precise parallax measurements obtained through pulse timing or interferometric techniques. Others result from H I absorption measurements combined with a kinematic rotation model for the Galaxy. Still others arise from the association of pulsars with supernova remnants and globular clusters. Distance estimates combined with dispersion measures quantify the line-of-sight average electron density. The new distance constraints indicate, in a minority of cases, that some of the distances derived from the TC93 model using pulsar dispersion measures are in error by factor of two or more. However, we point out that some of the parallax measurements also differ from previous ones by significant amounts. Additional information is provided by the distribution of dispersion measures for the entirety of available pulsar samples. The number of such measurements is about double of that available in 1993. Constraints on the square of the electron density arise from scattering measurements such as angular broadening, pulse broadening and diffractive

scintillation measurements. The number of scattering measurements has almost doubled since 1993.

The TC93 model is flawed in several respects, some of which were apparent even at the time of its development. First, it provides insufficient column density at high Galactic latitudes so that only lower bounds on pulsar distances can be derived from it. Second, in some directions, particularly in the fourth quadrant along tangents to the Carina-Sagittarius and Crux-Scutum spiral arms, the model provides either too many electrons for some objects (Johnston et al. 2001) or too few for others (as discussed below), indicating that the spiral arms need redefinition. Third, in the direction of the Gum Nebula and Vela supernova remnant, the TC93 model provides too little scattering to account for the pulse broadening of some pulsars (Mitra & Ramachandran 2001). Fourth, interstellar scintillations of nearby pulsars have scintillation bandwidths (which measure the column density of electron density fluctuations) that are not well modeled (Bhat & Gupta 2002). Fifth, similar to the first deficiency, the calibration between scattering of Galactic and extragalactic sources needs revision in order to ascertain the column density of scattering material toward cosmological sources as compared to that of Galactic objects outside of but near the apparent boundary of free electrons.

Our knowledge of the ISM has increased significantly from a host of other investigations across the electromagnetic spectrum. The local ISM, in particular, is now much better modeled and we incorporate that information into our model for the free electron density. The local ISM has been probed using continuum X-ray measurements and absorption of Na I toward nearby stars.

Other models for the mean electron density have been presented since TC93. These include the recent work of Gómez, Benjamin & Cox (2001; hereafter GBC01), who presented a two-component, axisymmetric model, not dissimilar in form to that used by Cordes et al. (1991). The two components have $\text{sech}^2(r/R)\text{sech}^2(z/H)$ variations with different radial and z scales. GBC01 do not attempt to model electron density fluctuations relevant to scattering and their model is based solely on the 109 objects available to them that have independent distance estimates. As we demonstrate, though their model is adequate for nearby pulsars, it grossly underpredicts the dispersion measures of many distant pulsars at low Galactic latitudes and some at high latitudes. Their work underscores the need, demonstrated before by others (Ghosh & Rao 1992; TC93), for spiral-arm structure in the free-electron distribution.

Our model uses significantly larger data samples than were available for TC93 and makes use of all available data, including independent distance constraints on pulsar distances, dispersion and scattering data on pulsars, and scattering of other Galactic as well as extragalactic sources. We also incorporate published, multiwavelength data that allows modeling of the local ISM and of the spiral arms of the Galaxy.

In this first paper we present the model and its usage. In a second paper (Cordes & Lazio 2002b; hereinafter Paper II) we describe the input data and associated references, the likelihood analysis and

modeling, alternative model possibilities, and discussions of particular lines of sight. Future papers will apply the model to various astronomical and astrophysical applications. The plan of this paper is as follows. In §2 we describe the observable quantities that we use to constrain the NE2001 model parameters. In §3 we describe the various components of the NE2001 model. In §4 we demonstrate the model's ability to account for the distances and scattering of pulsars and discuss briefly astronomical applications of the model. Extensive discussion of applications of NE2001 is deferred to a later paper.

In §5 we summarize the results and outline future prospects for improving the model. These will rest largely on usage of the Parkes Multibeam Pulsar sample (e.g. Manchester et al. 2001), improved parallax measurements using very long baseline interferometry, and incorporation of additional multiwavelength observations into the model definition and fitting. Appendix A describes our model for the local interstellar medium. Appendix B describes how to obtain the model as a set of Fortran subroutines and its implementation in tools available through the World Wide Web.

2. OBSERVABLES

In constructing the new model, we have used a variety of measurements, largely at radio wavelengths, but also including the results of optical and X-ray observations that probe various aspects of the local ISM. In this section we summarize the measurements used, defining line-of-sight integrated quantities in some detail because we provide expressions and software for estimating them using our model.

Radio data consist of measurements along particular lines of sight of propagation effects that are sensitive to the electron density and its fluctuations. In addition, there are independent distance estimates or constraints based on a variety of techniques (H I absorption, interferometric or timing parallaxes, and associations with globular clusters or supernova remnants). The wave-propagation data include: (a) dispersion measures (DMs) of pulsars obtained through measurements of differential arrival times; (b) temporal broadening of pulses from pulsars with large DM caused by multipath scattering from electron density variations, δn_e ; (c) scintillation bandwidth measurements of low-DM pulsars; (d) angular broadening of Galactic and extragalactic sources caused by scattering from δn_e ; and (e) emission measures.

In Table 1 we summarize the data sets by specifying the numbers of each kind of measurement. Figure 1 shows the relative number of measurements for pulsars.

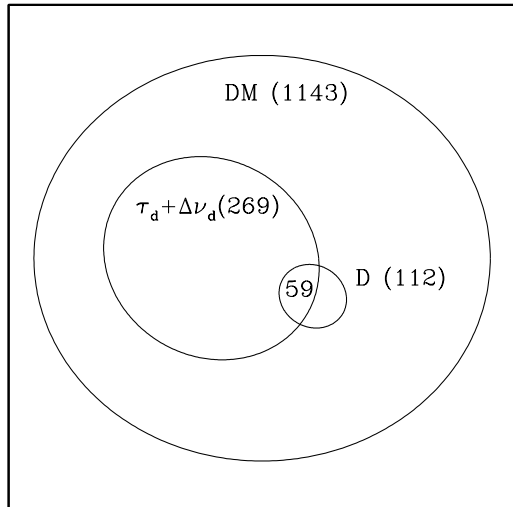


FIG. 1.— Venn diagram showing the number of DM measurements, independent distance measurements (D), scattering measurements (pulse broadening (τ_d) + scintillation bandwidth ($\Delta\nu_d$) measurements), and the overlap of pulsar distance and scattering measurements. In addition to pulsar data, there are 118 angular broadening measurements on non-pulsar Galactic sources and on 94 extragalactic sources. These numbers include upper limits. See Table 1 for additional information.

2.1. DM, EM, and Distance Measurements

The data used include 1143 dispersion measures,

$$\text{DM} \equiv \int_0^D ds n_e, \quad (1)$$

(Taylor, Manchester, & Lyne 1993; Princeton pulsar catalog; ¹ Parkes Multibeam survey ²).

We characterize distance constraints (e.g., from H I absorption measurements) with an interval $[D_L, D_U]$, where the lower and upper distance limits, D_L, D_U , are assumed to be hard limits, with uniform probability within the interval. A compilation with references is given on a web site. ³ The best distance constraints are from parallax measurements using pulse timing techniques (e.g. van Straten et al. 2001) and very-long-baseline interferometry (Chatterjee et al. 2001; Brisken et al. 2002).

The emission measure EM is the integral of the squared electron density,

$$\text{EM} = \int_0^D ds n_e^2, \quad (2)$$

and thus provides information about fluctuations in electron density and their spatial distribution.

2.2. Radio Wave Scattering Measurements

We use three kinds of measurements: the angular broadening (“seeing”) diameter θ_d ; the pulse broadening time, τ_d , that measures the temporal smearing associated with the multipath propagation; and the scintillation bandwidth, $\Delta\nu_d$, the frequency range over which diffractive scintillations are correlated. All three observables are sensitive to the detailed distribution along the line of sight of the scattering strength, owing to standard geometrical leveraging effects encountered in optics. Details are summarized below and discussed thoroughly in Cordes & Rickett (1998, hereafter CR98; see also Deshpande & Ramachandran 1998).

Angular broadening is characterized as the full-width at half-maximum (FWHM) of the scattering contribution to the measured brightness distribution.

The pulse broadening time τ_d is determined by deconvolving intrinsic and measured pulse shapes. The broadening times are roughly the e^{-1} time of the pulse broadening function, which is roughly a one-sided exponential (e.g., Cordes & Rickett 1998; Lambert & Rickett 1999).

The scintillation bandwidth ($\Delta\nu_d$) is estimated as the half-width at half maximum of the autocorrelation function of intensity along the frequency-lag axis (Cordes 1986; Johnston, Nicastro, & Koribalski 1998; Bhat, Rao, & Gupta 1999). The “uncertainty” relation between τ_d and $\Delta\nu_d$ may be written as $2\pi\Delta\nu_d\tau_d = C_1$, where C_1 is a constant that depends on the wavenumber spectrum and on the large-scale distribution of scattering material along the line of sight (CR98). We use $C_1 = 1.16$, the value appropriate for a uniform medium and having a Kolmogorov wavenumber spectrum.

2.2.1. Density Spectrum and Scattering Measure

We assume that $\delta n_e \propto n_e$ but with a proportionality constant that varies between different components of the Galactic plasma. Also, we adopt a power-law wavenumber spectrum for δn_e ,

$$P_{\delta n_e}(q) = C_n^2 q^{-\beta}, \quad \frac{2\pi}{\ell_0} \leq q \leq \frac{2\pi}{\ell_1}; \quad (3)$$

ℓ_1 and ℓ_0 are the inner and outer scales of the fluctuations in δn_e and C_n^2 is the spectral coefficient (the “level of turbulence”). We take $\beta = 11/3$, the “Kolmogorov” spectrum because it is appropriate for many lines of sight (e.g. Lee & Jokipii 1976; Armstrong, Rickett & Spangler 1995). We point out that there are numerous caveats on this choice of β , both empirical and theoretical, which we discuss in Paper II. ⁴ The scattering measure is the path integral of C_n^2 :

$$\text{SM} \equiv \int_0^D ds C_n^2. \quad (4)$$

Different observables correspond to different LOS weightings for C_n^2 , yielding different effective values for

¹

<http://pulsar.princeton.edu/pulsar/catalog.shtml>

²

<http://www.atnf.csiro.au/research/pulsar/pmsurv/>

³

<http://www.astro.cornell.edu/~shami/psrvlb/parallax.html>

⁴

Briefly, some observable quantities scale with frequency or distance differently than what is expected for a simple Kolmogorov model. Estimates of SM based on measured quantities may accordingly be in error. However, these errors are no more than a factor of a few and can be compared with line-of-sight variations of several orders of magnitude in SM that we aim to model.

the scattering measure. Following Cordes et al. 1991 and TC93, we define expressions for the *effective* SM if a uniform medium is assumed:

- (1) For measurements of angular diameters of extragalactic sources,

$$\text{SM}_{\theta,x} = \text{SM}. \quad (5)$$

- (2) For angular diameters of Galactic sources,

$$\text{SM}_{\theta,g} = 3 \int_0^D ds (1 - s/D)^2 C_n^2, \quad (6)$$

where the integration is from observer to source.

- (3) For pulse broadening and scintillation measurements,

$$\text{SM}_\tau = 6 \int_0^D ds (s/D)(1 - s/D) C_n^2. \quad (7)$$

With these expressions, the true SM for a statistically uniform medium would be estimated correctly. For nonuniform media, the results are only approximations to the true SM.

Under the same assumption of a uniform medium, we calculate observables in terms of these weighted SMs using (with ν in GHz and SM in units defined above):

$$\theta_d = \nu^{-11/5} \times \begin{cases} 128 \text{ mas SM}_{\theta,x}^{3/5} & \text{Extragalactic Sources} \\ 71 \text{ mas SM}_{\theta,g}^{3/5} & \text{Galactic Sources.} \end{cases} \quad (8)$$

The pulse broadening time and scintillation bandwidth are given by

$$\tau_d = 1.10 \text{ ms SM}_\tau^{6/5} \nu^{-22/5} D \quad (9)$$

$$\Delta\nu_d = 168 \text{ Hz SM}_\tau^{-6/5} \nu^{22/5} (C_1/1.16) D^{-1}. \quad (10)$$

The coefficient in Eq. 10 is the same as Eq. 48 of Cordes & Lazio (1991) if, as assumed there, $C_1 = 1.53$, the value appropriate for a medium with a square-law structure function. However, $C_1 = 1.16$ applies for a Kolmogorov medium that is statistically homogeneous and which we consider to be a better default model than a medium with square-law structure function.

Following Cordes et al. (1991) and TC93, we relate C_n^2 to the local mean electron density inside ionized clouds \bar{n}_e and calculate line of sight integrals taking into account the volume filling factor η of those clouds and cloud-to-cloud variations of the internal density. We use $n_e = \eta \bar{n}_e$ to denote the local spatially-averaged density. We relate SM to DM using

$$d\text{DM} = n_e ds, \quad (11)$$

$$d\text{SM} = C_{\text{SM}} F n_e^2 ds, \quad (12)$$

where F is a fluctuation parameter,

$$F = \zeta \epsilon^2 \eta^{-1} \ell_0^{-2/3}, \quad (13)$$

that depends on the fractional variance inside clouds, $\epsilon^2 = \langle (\delta n_e)^2 \rangle / \bar{n}_e^2$, the normalized second moment of cloud-to-cloud fluctuations in \bar{n}_e , $\zeta = \langle \bar{n}_e^2 \rangle / \langle \bar{n}_e \rangle^2$, and the outer scale ℓ_0 expressed in parsec units. We define the constant, $C_{\text{SM}} = [3(2\pi)^{1/3}]^{-1} C_u$, where the scale factor $C_u = 10.2 \text{ m}^{-20/3} \text{ cm}^6$ yields SM in the (unfortunately)

conventional units of $\text{kpc m}^{-20/3}$ for n_e in cm^{-3} , ds in kpc , and ℓ_0 in AU .

The emission measure may be expressed as

$$\begin{aligned} d\text{EM} &= [3(2\pi)^{1/3}] \ell_0^{2/3} \epsilon^{-2} (1 + \epsilon^2) d\text{SM} \\ &= 544.6 \text{ pc cm}^{-6} \ell_0^{2/3} \epsilon^{-2} (1 + \epsilon^2) d\text{SM}. \end{aligned} \quad (14)$$

For completeness, we provide expressions for the free-free optical depth, the related intensity of H α emission, and the transition frequency between weak and strong scattering. These quantities are evaluated using subroutines provided in the software described in Appendix B. The free-free optical depth is $\tau_{\text{ff}} = 5.47 \times 10^{-8} \nu^{-2} T_4^{-3/2} g(\nu, T) \text{EM}$ (ν in GHz, $T_4 =$ temperature in units of 10^4 K, and $g =$ Gaunt factor ~ 1) (Rybicki & Lightman 1979, p. 162). Relating EM to SM, we find that the implied free-free optical depth is

$$\tau_{\text{ff}} = 10^{-4.53} \nu^{-2} T_4^{-3/2} \nu^{-2} \ell_0^{2/3} \epsilon^{-2} (1 + \epsilon^2) \text{SM}. \quad (15)$$

The intensity of H α emission (in Rayleighs) in terms of SM (Haffner, Reynolds, & Tuftte 1998, Eq. 1) is

$$I_{\text{H}\alpha} = 198 R T_4^{-0.9} \epsilon^{-2} (1 + \epsilon^2) \ell_0^{2/3} \text{SM}. \quad (16)$$

The expression for the transition frequency between weak and strong scattering (Rickett 1990) used in the software discussed in Appendix B is

$$\nu_{\text{trans}} = 318 \text{ GHz } \xi^{10/17} \text{SM}^{6/17} D_{\text{eff}}^{5/17}, \quad (17)$$

where D_{eff} is now an effective distance to the scattering medium and the factor $\xi \sim 1$ allows scaling of one's preferred definition for the Fresnel scale (e.g. $\xi = (2\pi)^{-1/2}$ is commonly used, decreasing the coefficient by a factor 0.58). For spherical waves embedded in a medium with constant C_n^2 , the coefficient is multiplied by a factor $(\beta - 1)^{-2/(\beta+2)}$ and becomes 225 GHz. Thus, for nearby pulsars with $\log \text{SM} \approx -4$ and $D \approx 0.1$ kpc, $\nu_{\text{trans}} \approx 5$ GHz.

3. GALACTIC MODEL FOR ELECTRON DENSITY

3.1. Basic Structure

As in TC93, we use a right-handed coordinate system $\mathbf{x} = (x, y, z)$ with its origin at the Galactic center, x axis directed parallel to $l = 90^\circ$, and y axis pointed toward $l = 180^\circ$. The Galactocentric distance projected onto the plane is $r = (x^2 + y^2)^{1/2}$.

The electron density is the sum of two axisymmetric components and a spiral arm component, combined with terms that describe specific regions in the Galaxy. Table 2 gives the details of the functional forms, which we describe briefly here.

We have distinguished terms that represent the local ISM (n_{lism}), the large scale distribution (n_{gal}), the Galactic center (n_{GCC}), and individual clumps (n_{clumps}) and voids (n_{voids}). The large scale distribution, n_{gal} , consists of two axisymmetric components, a thick (1) and thin (2) disk, and spiral arms. The weight factor $w_{\text{lism}} = 0, 1$ switches off or on the local ISM component and switches on or off the smooth, large scale components of the model (and also the Galactic-center component, n_{GCC}). Superposed with the large-scale and local-ISM components are ‘‘clumps’’ of excess electron density that we infer from the database of measurements as outliers from the smooth model. They most likely correspond to individual H II

regions or portions of ionized shells surrounding supershell regions. Finally, we also include “voids” that generally are regions of lower than ambient density which are mutually exclusive of all components (except clumps) rather than superposing with them. Voids override all components other than clumps and are required to account for the distances of some pulsars.

Associated with each component in the model is a separate value of the fluctuation parameter, F . Details about the functions used are given in Table 2 and summarized in sections below. As in TC93, we use $\text{sech}^2(|z|/H)$ for the z dependences of most components to produce a “rounder” variation at $z = 0$ than an exponential dependence $\propto \exp(-|z|/H)$. Both the exponential and sech^2 functions integrate to the same asymptotic value (H) and have nearly equal $1/e$ locations.

Table 3 gives parameter values for the large scale parameters and compares them, where appropriate, with those of the TC93 model. The best-fitting parameters were found by an iterative likelihood analysis that is similar to that used in TC93 but with a number of improvements in the details of the fitting (Paper II).

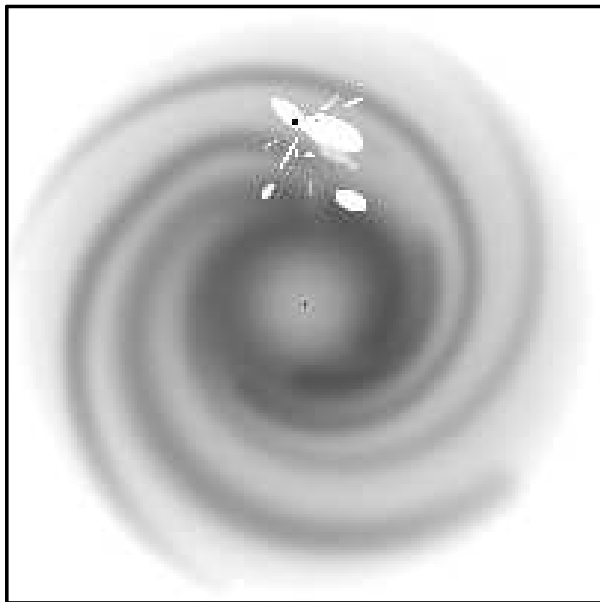


FIG. 2.— Electron density corresponding to the best fit model plotted as a grayscale with logarithmic levels on a 30×30 kpc x-y plane at $z=0$ and centered on the Galactic center. The most prominent large-scale features are the spiral arms, a thick, tenuous disk, a molecular ring component. A Galactic center component appears as a small dot. The small-scale, lighter features represent the local ISM and underdense regions required for by some lines of sight with independent distance measurements. The small dark region embedded in one of the underdense, ellipsoidal regions is the Gum Nebula and Vela supernova remnant.

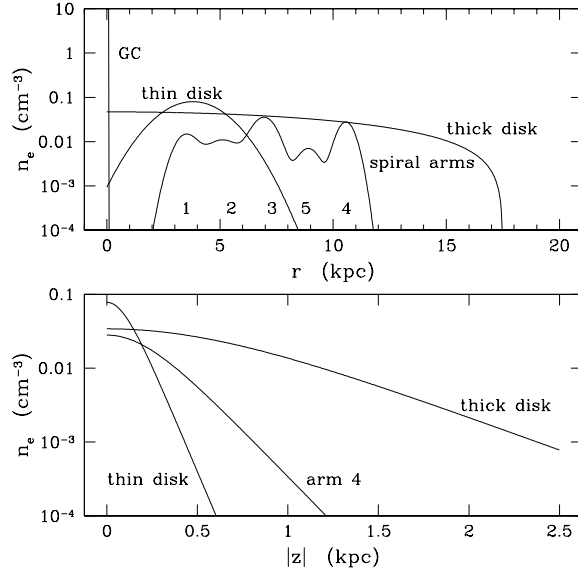


FIG. 3.— *Top*: Electron density plotted against Galactocentric radius in the direction from the Galactic center through the Sun for the various large-scale components. *Bottom*: Electron density plotted against $|z|$. For the inner Galaxy (thin disk) component, the profile is for $r = 3.5$ kpc, the peak of the annular component. For the thick disk component, the cut is at $r = R_\odot$. The spiral arm cut is at $(x, y) = 0, 10.6$ kpc.

3.1.1. Outer, Thick Disk Component

The outer, thick disk component is responsible for the DMs of globular cluster pulsars and the low-frequency diameters of high-latitude extragalactic sources (e.g., as inferred from interplanetary scintillation measurements). In TC93 this component was determined to have a scale height of roughly 1 kpc with a Galactocentric radial scale length of roughly 20 kpc. However, the data available for TC93 did not allow a firm constraint on the Galactocentric scale length; scale lengths as large as 50 kpc were also allowed by the data. Through measurements of scattering of extragalactic sources toward the Galactic anticenter, Lazio & Cordes (1998a,b) inferred a scale length ~ 20 kpc and a functional form that truncates at this scale. Alternatives are discussed in Paper II.

3.1.2. Inner, Thin Disk Component

An inner Galaxy component (n_2) consisted of a Gaussian annulus in TC93. Data available to TC93 could not distinguish a filled Gaussian form in Galactocentric radius from an annular form, but the latter was chosen for consistency with the molecular ring seen in CO (e.g., (Dame et al. 1987). We adopt the same form in our model; in Paper II we discuss alternatives to the annular form.

3.1.3. Spiral Arms

Is spiral arm structure required by pulsar dispersion measures and distance constraints? TC93 argue that it is by referring to the asymmetry of the distribution of DM vs. Galactic longitude (c.f. their Figure 2). The same asymmetry appears in the larger sample now available (Paper II). A direct demonstration can be made by calculating the DM deficit for individual pulsars for various electron-density models, defined as the difference between

the model DM integrated to infinite distance and the pulsar DM: $\Delta\text{DM} = \text{DM} - \text{DM}_\infty(\text{model})$. In Figure 4 we show ΔDM plotted against Galactic coordinates for the axisymmetric model of GBC01. There is a large number of DM deficits, both along the Carina-Sagittarius arm ($\ell \sim -65^\circ \pm 10^\circ$) and extending (at low latitudes) continuously to $\ell = +60^\circ$. This broad longitude range encompasses all of the spiral arms interior to the solar circle and the molecular ring. GBC01 identify the need for spiral structure in similar directions by comparing predicted and actual DMs for the much smaller data set they considered. The large number of deficits we identify with their model (183 out of 1143 objects) is a much stronger signal for spiral structure. Spiral arm structure appears to be mandatory in any electron density model that aspires to realism.

The TC93 model, though containing spiral structure, also has insufficient DM (Figure 5) along the Carina-Sagittarius arm and at high latitudes. The low latitude deficits are removed in the new model by redefining and refitting the spiral arms while the high latitude deficits are removed by refitting the outer, thick-disk component and the spiral arm scale heights.

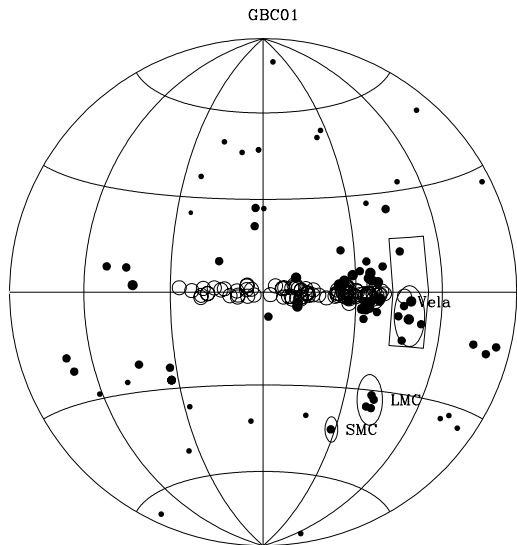


FIG. 4.— Plot of DM deficit, $\Delta\text{DM} = \text{DM} - \text{DM}_\infty(\text{GBC01})$ against Galactic coordinates, where $\text{DM}_\infty(\text{GBC01})$ is the maximum DM obtained by integrating the axisymmetric model of Gomez, Benjamin & Cox (2001; GBC01) to infinite distance. Longitudes 0° - 180° are on the left. Only positive residuals are shown, yielding 183 objects out of the 1143 pulsars in the combined Princeton and (public) Parkes Multibeam samples. The filled circles (going from smallest to biggest) represent $\Delta\text{DM} < 50$, $50 < \Delta\text{DM} \leq 200$, and $200 < \Delta\text{DM} \leq 400 \text{ pc cm}^{-3}$. The open circles are for $\Delta\text{DM} > 400 \text{ pc cm}^{-3}$. Ellipses designate pulsars in the Large and Small Magellanic Clouds and the Vela supernova remnant region. The rectangular region designates objects affected by the Gum Nebula. The GBC01 model is clearly deficient in a number of directions, including the cluster of objects near $(\ell, b) = -65^\circ \pm 10^\circ, 0^\circ$, which indicates insufficient column density along the Carina-Sagittarius spiral arm. A large number of objects have $\Delta\text{DM} > 0$ from longitudes -65° to $+60^\circ$, indicating the need for spiral structure in their model like that in TC93 and in the present model.

In the next version of the model, we will explore usage of a smaller Sun-GC distance.

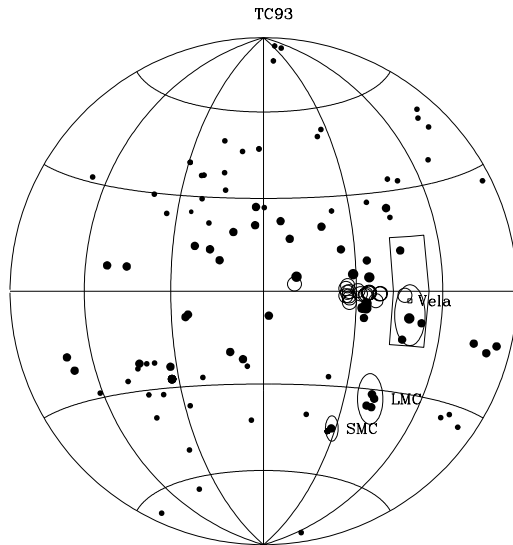


FIG. 5.— Plot of DM deficit, $\Delta\text{DM} = \text{DM} - \text{DM}_\infty(\text{TC93})$ against Galactic coordinates, where $\text{DM}_\infty(\text{TC93})$ is the maximum DM obtained by integrating the TC93 model to infinite distance. The format is the same as in Figure 4. The TC93 model is clearly deficient in a number of directions, 134 out of 1143 pulsars having values of DM too large to be accounted for, including the cluster of objects near $(\ell, b) = -65^\circ \pm 10^\circ, 0^\circ$, which indicates insufficient column density along the Carina-Sagittarius spiral arm. The new model corrects these deficiencies.

The spiral arm centroids in the new model are defined as logarithmic spirals with perturbed locations similar to those used in TC93. Centroid parameters are similar to those of Wainscoat et al. (1992). The spiral structure is similar to that proposed by Ghosh & Rao (1992) and also described by Vallée (1995, 2002). We have maintained usage of a Sun-Galactic Center distance of 8.5 kpc, the IAU recommended value, although recent work favors a smaller distance, $\sim 7.1 \pm 0.4 \text{ kpc}$ (e.g., Reid 1993; Olling & Merrifield 1998)⁵. Details are given in Paper II. The new model includes a local (Orion-Cygnus) spiral arm. Also, each arm has an individual centroid electron density, width, scale height and F parameter. Figure 6 shows the locations of spiral arms as defined in TC93 and as modified by us.

We emphasize that the spiral arm components in our model, like those in TC93, are modeled as overdense regions. Astrophysically, however, the enhanced star formation in spiral arms will produce underdensities as well as overdensities, as has been demonstrated by the identification of supershells. Though we have adopted spiral arms as overdense regions, to account for DM and SM we have had to introduce ellipsoidal underdense perturbations (“voids”) in particular directions (§3.6).

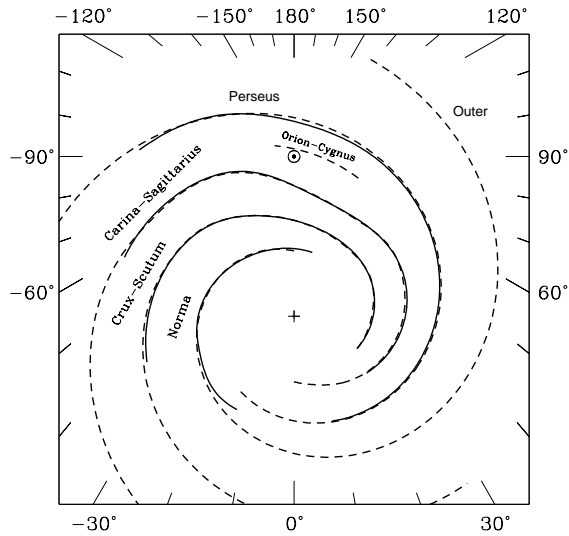


FIG. 6.— Solid lines: spiral model of the Galaxy used in TC93, defined according to work by Georgelin & Georgelin (1976), modified as in TC93. Dashed lines: a four-arm logarithmic spiral model combined with a local (to the Sun) arm using parameters from Table 1 of Wainscoat et al. (1992), but modified so that the arms match some of the features of the arms defined in TC93. The names of the spiral arms, as in the astronomical literature, are given. A + sign marks the Galactic center and the Sun is denoted by \odot .

3.2. Local ISM (LISM)

We model the local ISM in accord with DM and SM measurements of nearby pulsars combined with parallax measurements and guided by $H\alpha$ observations that provide estimates of EM. Observations and analysis by Heiles (1998), Toscano et al. (1999 and references therein), Snowden et al. (1998), Maíz-Apellíz (2001) and others (see Appendix A) suggest the presence of four regions of low density near the Sun: (1) a local hot bubble (LHB) centered on the Sun's location; (2) the Loop I component (North Polar Spur) that is long known because of its prominence in nonthermal continuum maps; (3) a local superbubble (LSB) in the third quadrant; and (4) a low density region (LDR) in the first quadrant. Additional features have been identified by Heiles (1998) but the available lines of sight to pulsars appear to not require their inclusion in our model. Bhat et al. (1999) explicitly fitted for parameters of the LHB using pulsar measurements and a model having a low-density structure surrounded by a shell of material that produces excess scattering. Some of the parallax distances used by Toscano et al. (1999) have been revised, in some cases substantially, implying lower densities in the third quadrant than they inferred.

Appendix A describes the mathematical models used for the four regions. Table 4 lists the parameters of the local ISM model and their values based on the fitting we describe in Paper II.

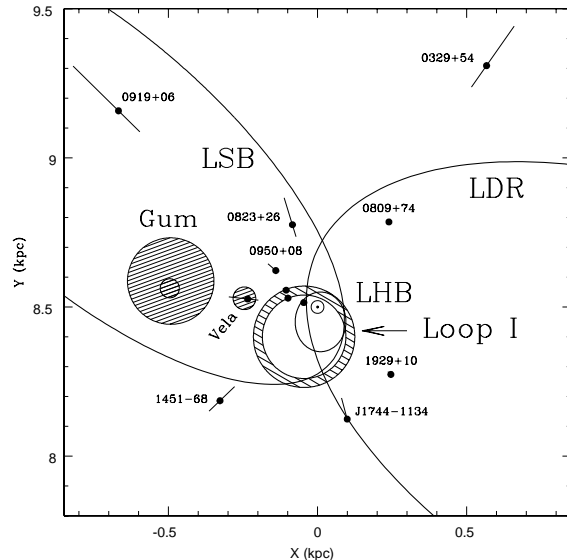


FIG. 7.— Projection onto the Galactic (X-Y) plane of the four local interstellar medium components, LHB, LSB, LDR and Loop I along with the clumps defining the Gum Nebula and the Vela supernova remnant. The LSB and LDR are the large ellipsoids, Loop I is the annular hatched region and the LHB is the small ellipsoid containing the Sun (\odot). Filled circles show the DM-predicted locations using NE2001 of those pulsars having parallax measurements. The lines plotted through each point (not all are visible) represent the allowed distance ranges from the parallax measurements. The three unlabeled points closest to the Sun are pulsars B1237+25, J0437-4715, and B1133+16 in order of increasing projected distance from the Sun.

3.3. Galactic Center (GC) Component

A new component is the region in the Galactic center that is responsible for scattering of Sgr A* and OH masers (van Langevelde et al. 1992; Rogers et al. 1994; Frail et al. 1994). Typical diameters, scaled to 1 GHz, are approximately $1''$, roughly 10 times greater than that predicted by TC93, even with the general enhancement of scattering toward the inner Galaxy in that model. The model of the region is based on work by Lazio & Cordes (1998c,d) who used angular sizes of extragalactic sources viewed through Galactic center to localize and model the region.

We use a slightly altered version of the axisymmetric model of Lazio & Cordes (1998d). We use a scale height $H_{GC} \approx 0.026$ kpc and slightly smaller radial scale, $R_{GC} \approx 0.145$ kpc. In addition we have offset the center of the distribution by $(x_{GC}, y_{GC}, z_{GC}) = (-0.01, 0, -0.02)$ kpc. The offset ellipsoid exponential is truncated to zero for arguments smaller than -1 . A value $F_{GC} \sim 6 \times 10^4$ produces SM values needed to account for the scattering diameters of Sgr A* and the OH masers.

3.4. Gum Nebula and Vela Supernova Remnant

In TC93 a large region was included which perturbed the dispersion measures of pulsars viewed through the Gum Nebula but did not influence the scattering. Since the writing of TC93, investigations of the Vela pulsar and other pulsars indicate that scattering is large within a region of at least 16 degrees diameter centered roughly on the direction of the Vela pulsar (Mitra & Ramachandran

2001). We have modeled the Gum/Vela region based on the scattering measurements and also on the fact that enhanced, local mean electron density is required to account for the dispersion measures and/or distances of five objects.

We model the direction toward the Gum Nebula with an overlapping pair of spherical regions describing the Gum Nebula itself and another for the immediate vicinity of the Vela pulsar. These are included in the list of “clumps” that enhance the electron density and F (see below).

3.5. Regions of Intense Scattering (“Clumps”)

In addition to regions that perturb the scattering of the Vela pulsar and other pulsars near it and the Galactic center, other regions of intense scattering must exist to account for the large angular diameters and/or pulse broadening seen toward a number of Galactic and extragalactic sources. We define “clumps” as regions of enhanced n_e or F or both and identify them by iterating with preliminary fits to the smooth components of the electron-density model (e.g., the thin and thick disk components and the spiral arms). Clumps are effectively manifestations of the Galaxy’s mesoscale structure not modeled adequately by the assumed large-scale components.

We model clumps with thickness $\Delta s \ll D$, and we use parameters $n_{e,c}$, F_c and d_c (electron density inside the clump, fluctuation parameter, and distance from Earth). The implied increments in DM and SM are

$$\begin{aligned} \text{DM}_c &= n_{e,c} \Delta s \\ \text{SM}_c &= C_{\text{SM}} F_c n_{e,c}^2 \Delta s = 10^{-5.55} \text{DM}_c^2 F_c / \Delta s_{\text{kpc}}, \end{aligned} \quad (18)$$

where the last equality holds for DM and SM in standard units. Equation 18 implies that relatively modest contributions to DM can produce large changes in SM if the clump is small and fluctuation parameter large. For example, $\text{DM}_c = 10 \text{ pc cm}^{-3}$, $F_c = 1$ and $\Delta s = 0.02 \text{ kpc}$ yield $\text{SM}_c = 0.014 \text{ kpc m}^{-20/3}$. For a pulsar 1 kpc away, the clump would perturb DM and the resultant distance estimate by perhaps 30% while SM would increase by about a factor of 100. Thus pulsars which have anomalous scattering relative to the smooth model can, in many cases, be well modeled with only small perturbations to the DM predictions of the model. This also means that the model is expected to be much better for distance and DM estimation than for scattering predictions.

Table 5 lists clumps needed to account for the scattering toward specific AGNs that have enhanced scattering; most are in the Cygnus region. Table 6 lists clumps needed to account for the scattering of non-pulsar Galactic sources; all are OH masers except for the Galactic continuum source Cyg X-3. For these non-pulsar sources, only the scattering is measured and so the clump perturbation, SM_c , is the most robustly determined clump parameter. We adopt reasonable — but non-unique — values for the clump distance, radius, and fluctuation parameter which imply a value for the clump’s DM_c , which we also tabulate.

For pulsar lines of sight, on the other hand, the clump’s contributions to both DM and SM are constrained if a scattering measurement exists. Included in Table 7 are those clumps that have $\text{DM}_c > 20 \text{ pc cm}^{-3}$ or $\text{SM}_c > 1 \text{ kpc m}^{-20/3}$. Operationally, the model includes additional,

weaker clumps that bring the scattering and distances into accord with observations. The software implementation of the model (see below) includes these weaker clumps as well as those listed in Tables 5–7.

In most cases our fitting procedure does not provide unambiguous distance estimates for the clumps. The distances listed in Tables 5–7 are “plausible” distance estimates for clumps, locating them, for instance, in or near spiral arms or in specific HII complexes that contain molecular masers.

3.6. Regions of Low Density (“Voids”)

We found that some pulsar distance constraints could not be satisfied using the previously defined structures without recourse to placement of a low-density region along the line of sight. We call these regions “voids” although they simply represent, typically, regions with lower-than-ambient density. By necessity, they take precedence over all other components (except clumps), which we effect by usage of a void weight parameter, $w_{\text{voids}} = 0, 1$, that operates similarly to w_{lism} . The mathematical form is given in Table 2. We use elliptical gaussian functions with semi-major and semi-minor axes a, b, c and a rotation angle θ_z about the z axis. Table 8 lists the properties of all voids used in the current realization of the model.

4. MODEL PERFORMANCE

The quality of the model can be evaluated on the basis of how well it estimates the distances and scattering of pulsars with appropriate measurements.

Figure 7 shows nearby pulsars with parallax distance ranges plotted as lines projected onto the Galactic plane. Extrapolations of these lines intersect the Sun’s location. The filled circles indicate the distance estimated with NE2001. As can be seen, distance estimates for most of the nearby pulsars are acceptable. A uniform medium or one with only large-scale structure (i.e. one without the Gum Nebula, Vela supernova remnant, and LISM components) would do much more poorly.

Figure 8 shows a projection onto the Galactic plane of distance ranges and model estimates for those pulsars having independent distance constraints and Galactic latitudes, $|b| < 5^\circ$. Only six objects have model distances that fall outside the distance range. As commented upon in Paper II two objects have questionable lower distance bounds from H I absorption. The other four lines of sight are toward pulsars in low-latitude globular clusters toward the Galactic center. Also shown in the figure along the perimeter (as filled squares) are objects for which the TC93 model could provide only a lower distance bound. These occur in the directions along the Carina-Sagittarius spiral arm, through the Gum Nebula, and toward the inner Galaxy near $\ell \approx -20^\circ$. The new model accounts for the DMs of these objects by having larger electron densities along the relevant lines of sight.

Figure 9 shows the DM-calculated distance plotted against independent distance constraints, $[D_L, D_U]$. Model estimates are bracketed by $[D_L, D_U]$ in the large majority of cases (90 of 120 total, though not all are plotted and some of the 30 non-bracketed cases are multiple pulsars in the same globular cluster). For most cluster pulsars,

the distance is underestimated because the cluster is well beyond the electron layer of the Galaxy.

Figure 10 quantifies the model’s ability to account for the scattering of known objects as a histogram of the quantity $r_{\text{scatt}} = (\text{predicted scattering})/(\text{measured scattering})$. The large peak centered on $r_{\text{scatt}} = 1$ indicates that most lines of sight are well modeled, though some outliers remain. The outliers are largely globular cluster pulsars whose distances are poorly estimated by the model and a few objects whose lines of sight are dominated by the local ISM. It should be emphasized that many of the small scale features in the present model were introduced to yield a good prediction of the scattering, so the histogram is largely a manifestation of our modeling approach. The predictive aspect of the model will be tested when it is applied to objects on which new scattering measurements are obtained.

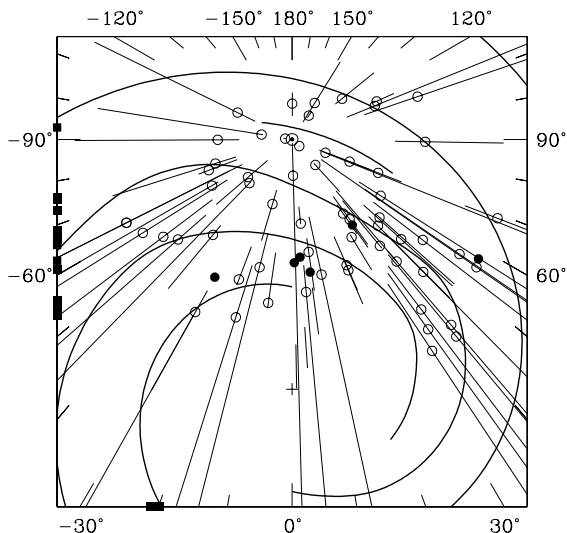


FIG. 8.— Distances calculated from model NE2001 projected onto the Galactic plane for objects with $|b| < 5^\circ$. In the interior of the box, plotted lines indicate independent distance ranges, $[D_L, D_U]$, open circles denote “good” fits (i.e. model distances \hat{D} that are within the empirical range) while the six filled circles designate pulsars where the model distance underestimates the minimum empirical distance. Two of these objects (B1930+22, $\ell = 57.4^\circ$, $b = 1.6^\circ$; J1602–5100, $\ell = -29.3^\circ$, $b = 1.3^\circ$) have uncertain lower distance bounds from HI absorption while the other four are globular cluster pulsars at low latitudes toward the Galactic center ($0^\circ \lesssim \ell \lesssim 40^\circ$). On the perimeter of the box, filled squares denote pulsars with $|b| \leq 5^\circ$ for which the TC93 model fails to yield distance estimates because their dispersion measures exceed those of the model: $DM > DM_\infty(\text{TC93})$. These points are at or near tangents to the spiral arms in the fourth quadrant ($-83^\circ \leq \ell \leq -67^\circ$) or are along the line of sight through the Gum Nebula. The new model corrects these defects and has $DM(\text{NE2001}) > DM$ for all objects except those in the Magellanic clouds.

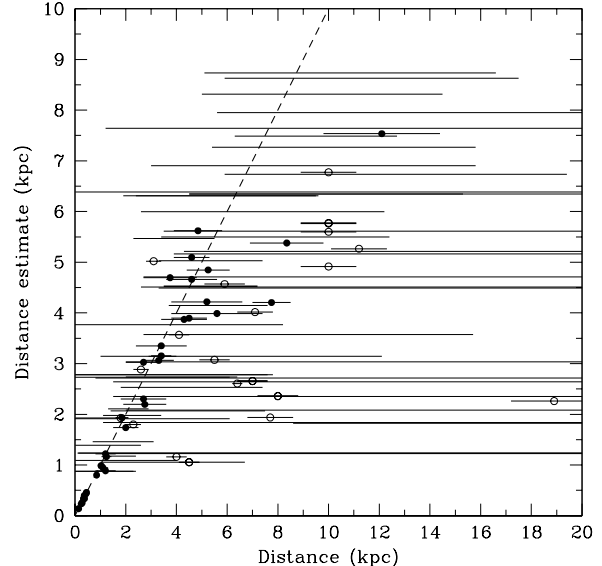


FIG. 9.— Distances calculated from the model plotted against independent empirical ranges, $[D_L, D_U]$, shown as horizontal lines. A filled circle is plotted at $(D_L + D_U)/2$ when the range is relatively small, $D_U/D_L < 2$. For globular cluster pulsars, an open circle is plotted.

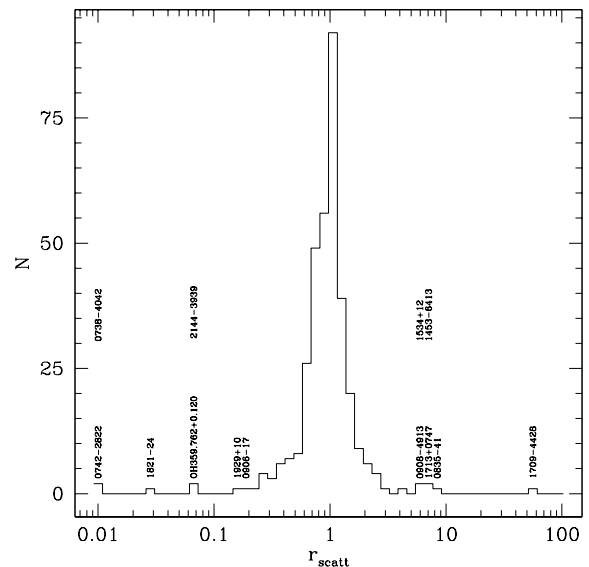


FIG. 10.— Histogram of the scattering prediction ratio, r_{scatt} , defined as $r_{\text{scatt}} = \text{predicted} / \text{actual}$ value of scattering observable for angular and pulse broadening and $r_{\text{scatt}} = \text{actual} / \text{predicted}$ for scintillation bandwidths. Thus $r_{\text{scatt}} > 1$ ($r_{\text{scatt}} < 1$) means scattering is overpredicted (underpredicted).

4.1. Asymptotic Values for DM

Figure 11 shows asymptotic values for DM in our model, DM_∞ , plotted against Galactic longitude. In the inner Galaxy, the asymptotic values exceed the highest known DM (1209 pc cm^{-3}) by a substantial factor. The lack of pulsars with such large values of DM is consistent with various selection effects, as we discuss in Paper II. For instance, the channel bandwidths used in the Parkes survey imply dispersion smearing of order 15 ms for $DM = 2000 \text{ pc cm}^{-3}$, comparable to the pulse width of many pulsars. More importantly, the pulse broadening from

scattering will exceed 1 s for many objects. Combined with inverse square law effects, one would not expect to find pulsars with much larger values of DM to be present in the existing surveys.

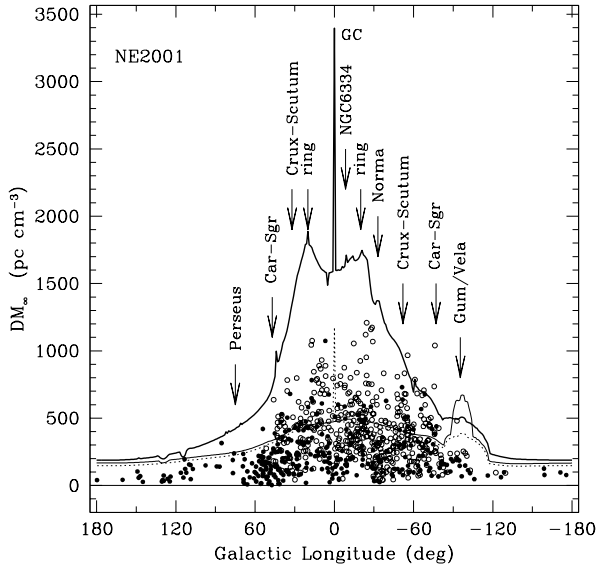


FIG. 11.— Plot of $DM_{\infty}(\ell, b)$, the maximum DM obtained by integrating the NE2001 model. Heavy solid line: $b = 0^\circ$. Light solid line: $b = -5^\circ$. Dotted line: $b = +5^\circ$ (offset by -20 pc cm^{-3} in the vertical direction for clarity). Plotted points are pulsars with $|b| < 5^\circ$. Filled circles: pulsars from the Princeton catalog. Open circles: pulsars from the public Parkes Multibeam catalog. Labelled features include tangents to the spiral arms and maxima associated with the ring component, the Gum Nebula and Vela supernova remnant, and the H II complex NGC 6334. The gaps near $\ell = +15^\circ$ and -20° and $DM \lesssim 200 \text{ pc cm}^{-3}$ are real, appearing in both samples, and signify either the real absence of pulsars in the corresponding volume or the presence of large electron densities in these directions fairly close to the solar system. The absence of pulsars above $\sim 1200 \text{ pc cm}^{-3}$ is due to selection against such objects by pulse broadening from dispersion smearing and scattering.

4.2. Distance Errors to be Expected

An ionized feature not included in our model will perturb the dispersion measure toward an individual object by an amount ΔDM . From the definition of DM, it follows that the consequent distance error, if small, will be

$$\Delta D = \frac{\Delta DM}{n_e(\mathbf{x}(D))}. \quad (19)$$

Thus, for given ΔDM , the distance error is larger for a pulsar in a region of small electron density compared to one in a dense region. (Of course, the perturbation can be large enough to render a very large distance error not describable by Eq. 19.) A particularly important case is for an object that is more than one scale height above the Galactic disk. Using a simple plane-parallel model as an example, the distance error is

$$\Delta D = \frac{\Delta DM}{n_{e0}(1 - DM/DM_{\infty})}, \quad (20)$$

where $DM_{\infty} = n_{e0}H/\sin|b|$ is the maximum DM of the model with midplane density n_{e0} and scale height H toward a direction at Galactic latitude b . For objects with

DM near the asymptotic value, distance errors are much larger than for objects within one scale height of the plane. This is true for both positive and negative perturbations from density enhancements and voids, respectively. For large positive perturbations of DM the measured DM can exceed DM_{∞} (or its analog in our multicomponent model). In this case, the model can yield only a lower bound on the distance.

For NE2001, we have explicitly constructed the model so that nearly all known pulsars have $DM < DM_{\infty}$. This feature may introduce bias in the model because there very well could be pulsars at large distances with DMs that are small because an unmodeled void is present along the line of sight. We estimate that the number of lines of sight for which this would be true is a small fraction of the total pulsar sample.

In Figure 12 we show the distance errors that ensue when we perturb DM by amounts corresponding to H II regions of different kinds. For reference, we expect perturbations in DM with the following amplitudes (e.g. Prentice & ter Haar 1969; Bronfman et al. 2000):

1. Strömgen sphere around an O5 star: $\Delta DM \approx 75 \text{ pc cm}^{-3}$.
2. Strömgen sphere around an O9/B1 star: $\Delta DM \approx 3 \text{ to } 10 \text{ pc cm}^{-3}$.
3. OB association: $\Delta DM \approx 100 \text{ to } 200 \text{ pc cm}^{-3}$.
4. Ultra-compact H II region: $\Delta DM \approx 300 \text{ to } 500 \text{ pc cm}^{-3}$. Through a simulation of pulsar and UCHII regions born in spiral arms and the molecular ring, we find that one expects only about one pulsar out of the observed population to intersect an UCHII region.

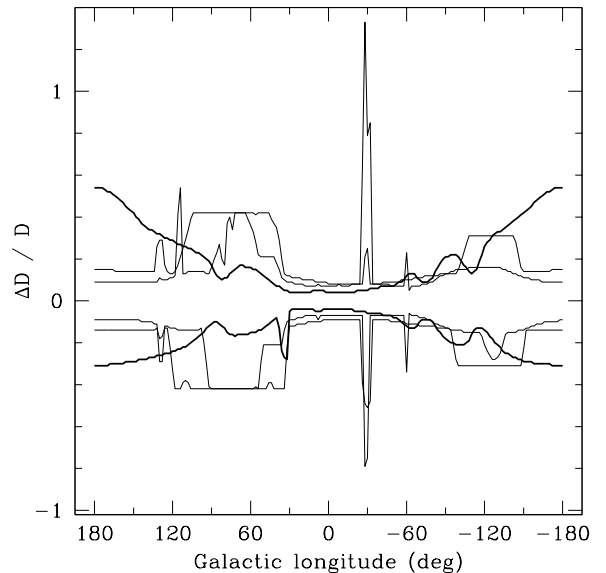


FIG. 12.— Plot of fractional distance error, $\Delta D/D$, against Galactic longitude where $\Delta D = \hat{D} - D$. The curves are calculated for perturbations to DM of $\pm \Delta DM$ which increase or decrease the model distance, \hat{D} , from the actual distance. Thickest line: $D = 5 \text{ kpc}$ and $\Delta DM = 30 \text{ pc cm}^{-3}$. Medium line: $D = 2 \text{ kpc}$ and $\Delta DM = 10 \text{ pc cm}^{-3}$. Thinnest line: $D = 1 \text{ kpc}$ and $\Delta DM = 5 \text{ pc cm}^{-3}$.

4.3. Comparison with TC93 Distances

Figure 13 compares distance estimates from NE2001 with those from TC93. The general trend is that the TC93 distances are larger, in some cases significantly so, than NE2001 distances; there are also cases where NE2001 provides smaller distances. The generally larger TC93 distances are consistent with our other diagnostics, which signify that TC93 provides too few electrons along many lines of sight. As designated in the figure, TC93 fails to give a distance estimate for 134 lines of sight. The smaller distances from NE2001 will influence estimates of pulsar space velocities and luminosities.

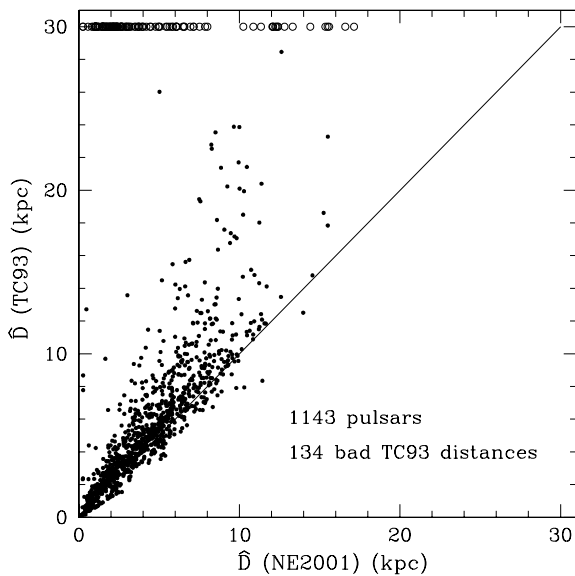


FIG. 13.— Distance estimates from NE2001 plotted against those from TC93. Filled circles designate objects for which both models yield a distance estimate. Open circles plotted at the top of the frame designate the 134 pulsars for which TC93 gives only lower distance estimates. The solid line shows equality of the two distance estimates.

4.4. Applications

To illustrate model predictions we show the model DM for lines of sight in the Galactic plane ($b = 0$) in Figure 14. Figure 15 shows DM plotted against Galactic coordinates in an Aitoff project when integrating the electron density to infinite distance. A similar pair of plots for SM is shown in Figures 16 and 17.

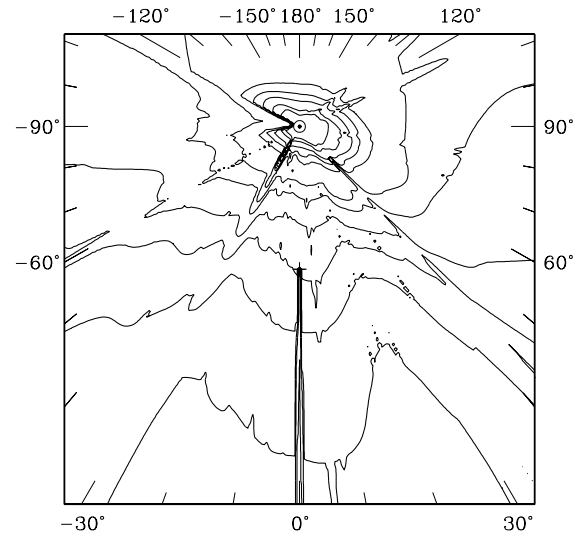


FIG. 14.— Contours of DM plotted on the Galactic plane. Contours are at 20, 30, 50, 70, 100, 200, 300, 500, 700, 1000, 1500, 2000, 3000 and 4000 pc cm^{-3} , with the lowest contour nearest the Sun (\odot), assumed to be 8.5 kpc from the Galactic center (+ symbol at plot center).

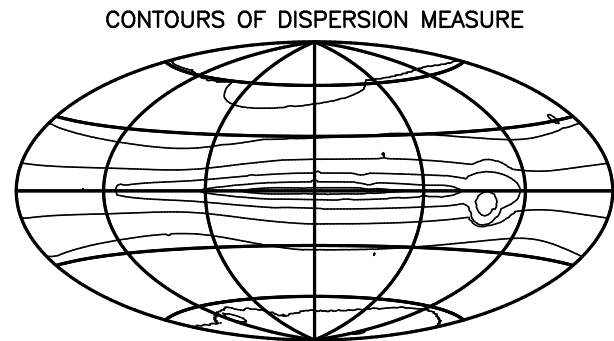


FIG. 15.— Contours of DM integrated to infinite distance and plotted against Galactic latitude and longitude on an Aitoff projection with the Galactic center in the middle and negative longitudes to the right. Contours are at $4000/2^n$ pc cm^{-3} for $n = 0, 1, \dots, 7$, with the lowest contour at the Galactic poles.

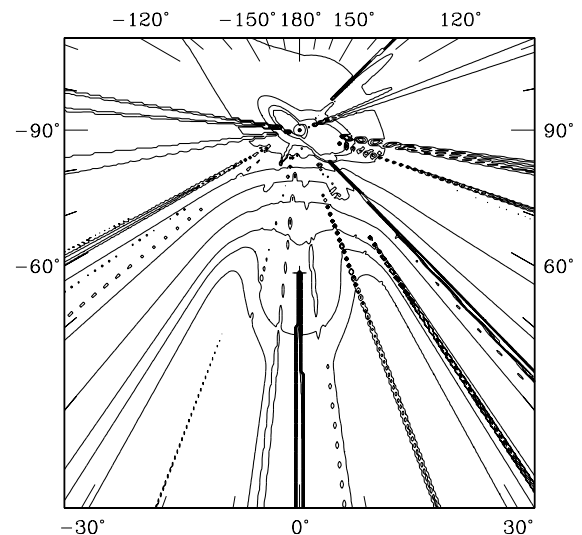


FIG. 16.— Contours of $\log SM$ plotted on the Galactic plane. Contours are at $\log SM = -5, -4, -3, -3, -2, -1, 0, 0.50, 0.67, 0.83, 1, 2, 3, 4, 5,$ and $6 \text{ kpc m}^{-20/3}$, chosen to bring out salient features. The lowest contour is near the Sun (\odot). SM is influenced much more than DM by small scale features in the model.

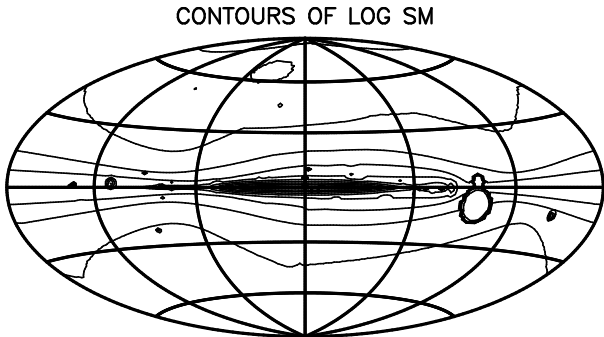


FIG. 17.— Contours of $\log SM$ integrated to infinite distance and plotted against Galactic latitude and longitude on an Aitoff projection with the Galactic center in the middle and negative longitudes to the right. Contours are at $4 - n/2 \text{ kpc m}^{-20/3}$ for $n = 0, 1, \dots, 16$, with the lowest contour at the North Galactic pole.

5. SUMMARY & CONCLUSIONS

We have presented a new model, NE2001, for the Galactic distribution of free electrons and the fluctuations within it. As observational constraints we make use of pulsar dispersion measures and distances and radio-wave scattering measurements available at the end of 2001 (hence its name), and we are guided by multi-wavelength observations of the Galaxy, particularly of the local interstellar medium.

Building on the Taylor-Cordes model (TC93), we model the free electron distribution as composed of three large-scale components, a thick disk, thin disk, and spiral arms. Since the publication of the TC93 model, though, the number of available data have expanded greatly (e.g., the number of pulsar DMs available is now approximately double the number available to TC93). With this larger data set, it is clear that “smooth,” large-scale components are insufficient to produce a realistic description of the electron density distribution. We must take into account the distribution of electrons in the local ISM, and we require “clumps” and “voids” of electrons, mesoscale structures distributed throughout the Galaxy on a large number of lines of sight in order to produce reasonable agreement with the observations.

Tables 2–4 summarize the model and the best-fitting parameters of the large-scale and local ISM components. Tables 5–8 lists the lines of sight requiring clumps or voids and the relevant parameter for each clump or void. Figure 2 shows the model electron density in the Galactic plane.

We used an iterative likelihood method to find the best-fitting model parameters. Our focus here has been on the exposition of the model. In a companion paper (Cordes & Lazio 2002b) we describe details of the fitting procedure and discuss those lines of sight that require a clump or void or are otherwise problematic. We also discuss possible alternative fitting approaches and models.

Our model, NE2001, improves upon the TC93 model. First, the distance estimates obtained from the model agree with available distance constraints for nearly

all pulsars with such constraints. Second, none of the parameters of the large-scale components are indeterminate (e.g., as was the case with the thick disk for TC93). The cost of these improvements has been an increase in the complexity of the model, particularly with respect to the number and location of clumps and voids. We believe, however, that this additional complexity is justified both by the quantity of data and because it is astrophysically reasonable. A small number of pulsars or extragalactic sources has been known for some time to have anomalously large DMs or scattering properties or both due to intervening H II regions or supernova remnants.

While we consider NE2001 to be an improvement over TC93, we foresee a number of probable developments that will allow future generations of electron density models. We group these improvements into increases in the quantity of data and improvements in the modeling technique. Perhaps most important will be an increase in the number of pulsar parallaxes, both from pulse timing methods applied to millisecond pulsars and from large programs using very long baseline interferometry (VLBI). Also, using pulsar luminosities to estimate distances should become feasible once beaming of pulsar radiation becomes better understood and despite the fact that the luminosity function for radio emission from pulsars is very broad. DM-independent distances provide crucial calibration information for NE2001 or any successors, and we regard it as likely that the number of pulsars with DM-independent distances will double in the next few years. We have made use of only the positions and DMs of pulsars discovered in the Parkes multibeam sample. Efforts are underway to measure the scattering along the lines of sight to many of these pulsars, which could increase the number of lines of sight with measured SMs by roughly 50% or more. The advent of the Green Bank Telescope and the refurbished Arecibo telescope suggest the possibility of conducting a northern hemisphere equivalent of the Parkes multibeam sample, which could increase the number of pulsars by at least another 50%.

Possible improvements in modeling include the adoption of a more realistic location for the Sun. NE2001 places the Sun in the Galactic plane at a Galactocentric distance of 8.5 kpc, though a smaller distance from the Galactic center ($\approx 7.1 \text{ kpc}$) and a modest offset from the plane ($\approx 20 \text{ pc}$) seem warranted. Although we have provided a formalism for comparing DM and SM to EM, we have made little use of it. Future work to include observational constraints on EM, e.g., from H α surveys, has the potential of producing a better model for the local ISM.

Finally, Figure 11 suggests that the large-scale structure of the Galaxy could be determined *ab initio*, provided that a sufficient number of lines of sight exist. Rather than imposing a large-scale structure as done both here and previously, the presence and location of large-scale components, particularly the spiral arms, could be determined directly from the population of pulsars. Future pulsar surveys may yield the number of lines of sight required to employ this approach.

We thank Z. Arzoumanian, R. Bhat, F. Camilo, S. Chatterjee, D. Chernoff, M. Goss, Y. Gupta, S. Johnston,

F. J. Lockman, R. N. Manchester, and B. Rickett for useful discussions. Our research is supported by NSF grant AST 9819931 and by the National Astronomy and Ionosphere Center, which operates the Arecibo

Observatory under cooperative agreement with the NSF. Basic research in radio astronomy at the NRL is supported by the Office of Naval Research.

REFERENCES

- Armstrong, J. W., Rickett, B. J. & Spangler, S. R. 1995, *ApJ*, 443, 209
 Berkhuijsen, E. M., Haslam, C. G. T., & Salter, C. J. 1971, *A&A*, 14, 252
 Bhat, N. D. R. & Gupta, Y. 2002, *ApJ*, 567, 342
 Bhat, N. D. R., Rao, A. P., & Gupta, Y. 1999, *ApJS*, 121, 483
 Brisken, W. F., Benson, J. M., Goss, W. M., & Thorsett, S. E. 2002, *ApJ*, 571, 906 (See also Brisken, W. F. 2001, Ph.D. Thesis, Princeton University.)
 Bronfman, L., Casassus, S., May, J., & Nyman, L.-Å. 2000, *A&A*, 358, 521
 Chatterjee, S., Cordes, J. M., Lazio, T. J. W., Goss, W. M., Fomalont, E. B., & Benson, J. M. 2001, *ApJ*, 550, 287.
 Cordes, J. M. 1986, *ApJ*, 311, 183
 Cordes, J. M. & Lazio, T. J. W. 2002b, *ApJ*, submitted (Paper II)
 Cordes, J. M. & Lazio, T. J. W. 1991, *ApJ*, 376, 123
 Cordes, J. M., Weisberg, J. M., Frail, D. A., Spangler, S. R., and Ryan, M. 1991, *Nature*, 354, 121
 Cordes, J. M., Weisberg, J. M., & Boriakoff, V. 1985, *ApJ*, 288, 221
 Cordes, J. M. & Rickett, B. R. 1998, *ApJ*, 507, 846 (CR98)
 Dame, T. M., et al. 1987, *ApJ*, 322, 706
 Deshpande, A. A. & Ramachandran, R. 1998, *MNRAS*, 300, 577
 Frail, D. A., Diamond, P. J., Cordes, J. M., & van Langevelde, H. J. 1994, *ApJ*, 427, L43
 Georgelin, Y. M. and Georgelin, Y. P. 1976, *A&A*, 49, 57
 Ghosh, T. & Rao, A. P. 1992, *A&A*, 264, 203
 Gómez, G. C., Benjamin, R. A., & Cox, D. P. 2001, *AJ*, 122, 908 (GBC01)
 Haffner, L. M., Reynolds, R. J. & Tufte, S. L. 1998, *ApJ*, 501, L83
 Heiles, C. 1998, *ApJ*, 498, 689
 Johnston, S., Koribalski, B., Weisberg, J. M., & Wilson, W. 2001, *MNRAS*, 322, 715
 Johnston, S., Nicastro, L., & Koribalski, B. 1998, *MNRAS*, 297, 108
 Lambert, H. C. & Rickett, B. J. 1999, *ApJ*, 517, 299
 Lazio, T. J. W. & Cordes, J. M. 1998a, *ApJS*, 115, 225 (LC98a)
 Lazio, T. J. W. & Cordes, J. M. 1998b, *ApJ*, 497, 238 (LC98b)
 Lazio, T. J. W. & Cordes, J. M. 1998c, *ApJS*, 118, 201 (LC98c)
 Lazio, T. J. W. & Cordes, J. M. 1998d, *ApJ*, 505, 715 (LC98d)
 Lee, L. C. & Jokipii, J. R. 1976, *ApJ*, 206, 735.
 Maíz-Apellániz, J. 2001, *ApJ*, 560, L83
 Manchester, R. N. et al. 2001, *MNRAS*, 328, 17
 Mitra, D. & Ramachandran, R. 2001, *A&A*, 370, 586
 Olling, R. P. & Merrifield, M. R. 1998, *MNRAS*, 297, 943
 Prentice, A. J. R. and ter Harr, D. 1969, *MNRAS*, 146, 423.
 Reid, M. J. 1993, *ARA&A*, 31, 345
 Rickett, B. J. 1990, *ARA&A*, 28, 561
 Rogers, A. E. E. et al. 1994, *ApJ*, 434, L59
 Rybicki, G. B. & Lightman, A. P. 1979, *Radiative Processes in Astrophysics* (Wiley: New York)
 Sfeir, D. M., Lallement, R., Crifo, F. & Welsh, B. Y. 1999, *A&A*, 346, 785
 Snowden, S. L., et al. 1998, *ApJ*, 493, 715
 Spoelstra, T. A. T. 1972, *A&A*, 21, 61
 Taylor, J. H. and Cordes, J. M. 1993, *ApJ*, 411, 674 (TC93)
 Taylor, J. H.; Manchester, R. N.; Lyne, A. G. 1993, *ApJS*, 88, 529
 Toscano, M., Britton, M. C., Manchester, R. N., Bailes, M., Sandhu, J. S., Kulkarni, S. R., & Anderson, S. B. 1999, *ApJ*, 523, L171
 Vallée, J. P. 1995, *ApJ*, 454, 119
 Vallée, J. P. 2002, *ApJ*, 566, 261
 van Langevelde, H. J., Frail, D. A., Cordes, J. M., & Diamond, P. J. 1992, *ApJ*, 396, 686
 van Straten, W., Bailes, M., Britton, M., Kulkarni, S. R., Anderson, S. B., Manchester, R. N., & Sarkissian, J. 2001, *Nature*, 412, 158
 Vergely, J.-L., Freire F. R., Siebert, A., & Valette, B. 2001, *A&A*, 366, 1016
 Wainscoat, R. J., Cohen, M., Volk, K., Walker, H. J., and Schwartz, D. E. 1992, *ApJS*, 83, 111

TABLE 1
DATA SUMMARY

Work	Number of Measurements					
	D ^a	DM	τ_d	$\Delta\nu_d$	$\theta_{d,\text{Gal}}$	$\theta_{d,\text{xgal}}$
TC93	74	553	120	74	38	42
This paper	112	1143	159	110	118	94

^aThe number of distances is the number of distinct lines of sight. A globular cluster with multiple pulsars is counted as only one line of sight.

TABLE 2
NE2001 MODEL COMPONENTS
 $n_e(\mathbf{x}) = (1 - w_{\text{voids}})\{(1 - w_{\text{lism}})[n_{\text{gal}}(\mathbf{x}) + n_{\text{GC}}(\mathbf{x})] + w_{\text{lism}}n_{\text{lism}}(\mathbf{x})\} + w_{\text{voids}}n_{\text{voids}}(\mathbf{x}) + n_{\text{clumps}}(\mathbf{x})$

Component	Functional Form	Parameters	No. Parameters	Comments
Smooth Components	$n_{\text{gal}}(\mathbf{x}) = [n_1 G_1(r, z) + n_2 G_2(r, z) + n_a G_a(\mathbf{x})]$			
Thick Disk	$n_1 G_1(r, z) = n_1 g_1(r) h(z/H_1)$	n_1, H_1, A_1, F_1	4	
Thin Disk	$n_2 G_2(r, z) = n_2 g_2(r) h(z/H_2)$	n_2, H_2, A_2, F_2	4	
Spiral Arms	$n_a G_a(\mathbf{x})$	$f_j n_a, h_j H_a, w_j w_a, F_j$ $j = 1, \dots, 5$	20	
Galactic Center (n_{GC})	$n_{\text{GC}0} e^{-[\delta r_{\perp}^2/R_{\text{GC}}^2 + (z - z_{\text{GC}})^2/H_{\text{GC}}^2]}$ $\delta r_{\perp}^2 = (x - x_{\text{GC}})^2 + (y - y_{\text{GC}})^2$	$n_{\text{GC}0}, R_{\text{GC}}, h_{\text{GC}}$	3	
Local ISM (n_{lism})	$n_{\text{lism}}(\mathbf{x}), F_{\text{lism}}(\mathbf{x}), w_{\text{lism}}(\mathbf{x})$ See below & Appendix A	See Table 4	36	Excludes Gum, Vela
Clumps (n_{clumps})	$\sum_{j=1}^{N_{\text{clumps}}} n_{c_j} e^{- \mathbf{x} - \mathbf{x}_{c_j} ^2/r_{c_j}^2} t_{c_j}(\mathbf{x})$	N_{clumps} $n_{c_j}, \mathbf{x}_{c_j}, r_{c_j}, F_{c_j}$	$6N_{\text{clumps}} + 1$ (6/clump)	Includes Gum, Vela
Voids (n_{voids})	$\sum_{j=1}^{N_{\text{voids}}} n_{v_j} g_v(\mathbf{x}; \boldsymbol{\theta}_{v_j}) t_{v_j}(\mathbf{x})$	N_{voids} $n_{v_j}, \mathbf{x}_{v_j}, \boldsymbol{\theta}_{v_j}, F_{v_j}$	$8N_{\text{voids}} + 1$ (8/void)	

Functions:

$$h(x) = \text{sech}^2(x)$$

$U(x)$ = unit step function

$$g_1(r) = [\cos(\pi r/2A_1)/\cos(\pi R_{\odot}/2A_1)]U(r - A_1)$$

$$g_2(r) = \exp(-(r - A_a)^2/A_a^2)U(r)$$

$$G_a(\mathbf{x}) = \sum_j f_j g_{a_j}(r, s_j(\mathbf{x})/w_j w_a) h(z/h_j h_a)$$

$s_j(\mathbf{x})$ tabulated

$$g_{a_j}(\mathbf{x}) = e^{-(s_j(\mathbf{x})/w_j w_a)^2} \text{sech}^2(r - A_a)/2U(r - A_a)$$

$$n_{\text{lism}}(\mathbf{x}) = (1 - w_{\text{lhb}})\{(1 - w_{\text{loopI}})[(1 - w_{\text{lhb}})n_{\text{ldr}}(\mathbf{x}) + w_{\text{lhb}}n_{\text{lhb}}(\mathbf{x})] + w_{\text{loopI}}n_{\text{loopI}}(\mathbf{x})\} + w_{\text{lhb}}n_{\text{lhb}}(\mathbf{x})$$

$$F_{\text{lism}}(\mathbf{x}) = (1 - w_{\text{lhb}})\{(1 - w_{\text{loopI}})[(1 - w_{\text{lhb}})F_{\text{ldr}}(\mathbf{x}) + w_{\text{lhb}}F_{\text{lhb}}(\mathbf{x})] + w_{\text{loopI}}F_{\text{loopI}}(\mathbf{x})\} + w_{\text{lhb}}F_{\text{lhb}}(\mathbf{x})$$

$$w_{\text{lism}}(\mathbf{x}) = \max[w_{\text{ldr}}(\mathbf{x}), w_{\text{lhb}}(\mathbf{x}), w_{\text{lhb}}(\mathbf{x}), w_{\text{loopI}}(\mathbf{x})] = (0, 1)$$

LISM weight function
truncation function

$$t_{c_j}(\mathbf{x}) = [1 - e_{c_j}U(|\mathbf{x} - \mathbf{x}_{c_j}| - r_{c_j})], \quad e_{c_j} = (0, 1)$$

$$g_v(\mathbf{x}, \boldsymbol{\theta}_{v_j}) = \text{elliptical gaussian} = \exp(-Q(\mathbf{x} - \mathbf{x}_{c_j})), \quad \boldsymbol{\theta}_{v_j} = (a_j, b_j, c_j, \theta_{y_j}, \theta_{z_j})$$

$$t_{v_j}(\mathbf{x}) = [1 - e_{v_j}U(Q - 1)], \quad e_{v_j} = (0, 1)$$

truncation function

$$Q = (\mathbf{x} - \mathbf{x}_{c_j})^\dagger \mathbf{V}^{-1}(\mathbf{x} - \mathbf{x}_{c_j}), \quad V = \text{rotation matrix}$$

ellipsoidal quadratic form
weight function for voids

$$w_{\text{voids}} = (0, 1)$$

Weight functions:

$w_{\text{voids}}, w_{\text{lism}}, w_{\text{ldr}}, w_{\text{lhb}}, w_{\text{lhb}}, w_{\text{lhb}}, w_{\text{loopI}}$ switch components on and off.

Truncation functions:

t_{c_j}, t_{v_j} truncate component at 1/e point if $e_{c_j}, e_{v_j} = 1$.

TABLE 3
PARAMETERS OF LARGE SCALE COMPONENTS OF TC93 AND NE2001

Parameter	TC93 Values	NE2001 Values ^a
$n_1 h_1$ (cm ⁻³ kpc)...	0.0165 ± 0.0006	0.033
h_1 (kpc)	0.88 ± 0.06	0.95
A_1 (kpc)	≥ 20	17
F_1	0.36 ^{+0.30} _{-0.10}	0.20
n_2 (cm ⁻³)	0.10 ± 0.03	0.090
h_2 (kpc)	0.15 ± 0.05	0.14
A_2 (kpc)	3.7 ± 0.3	3.7
F_2	43 ⁺³⁰ ₋₁₃	110
$n_a f_j$ (cm ⁻³)	0.084 ± 0.008	0.030 × (0.50, 1.2, 1.3, 1.0, 0.25)
$h_a h_j$ (kpc)	0.3 ± 0.1	0.25 × (1.0, 0.8, 1.3, 1.5, 1.0)
$w_a w_j$ (kpc)	0.3	0.6 × (1, 1.5, 1, 0.8, 1)
A_a (kpc)	8.5	11.0
$F_a F_j$	6 ⁺⁵ ₋₂	10 × (1.1, 0.3, 0.4, 1.5, 0.3)
n_G (cm ⁻³)	0.25	...
F_G	0.0	...
n_{GC} (cm ⁻³)	10.0
F_{GC}	5 × 10 ⁴

TABLE 4
LOCAL ISM COMPONENTS

Component	Location			Size & Shape				Density	
	\bar{x} (kpc)	\bar{y} (kpc)	\bar{z} (kpc)	a (kpc)	b (kpc)	c (kpc)	θ^a (deg)	n_e (cm ⁻³)	F
LDR	1.36	8.06	0.0	1.5	0.75	0.5	-24.8	0.012	0.1
LHB	0.01	8.45	0.17	0.085	0.1	0.33	15	0.005	0.01
LSB	-0.75	9.0	-0.05	1.05	0.425	0.325	139	0.016	0.01

Loop I (NPS)	Location			Size		Density			
	\bar{x} (kpc)	\bar{y} (kpc)	\bar{z} (kpc)	r (kpc)	Δr (kpc)	n_e (cm ⁻³)	Δn_e (cm ⁻³)	F_{vol}	F_{shell}
	-0.045	8.4	0.07	0.14	0.03	0.0125	0.010	0.20	0.01

^aFor LSB and LDR, θ is the angle of the major axis of the ellipsoid with respect to the the x axis ($\ell = 90^\circ$), increasing counterclockwise looking down on the Galactic plane. For the LHB, θ is measured from the z axis and describes the slant of the axis of the cylinder in the y - z plane. Loop I has a hemispherical shape with internal volume and shell component that contributes only for $z \geq 0$.

TABLE 5
CLUMP PARAMETERS FOR LINES OF SIGHT TO EXTRAGALACTIC SOURCES

LOS	ℓ (deg)	b (deg)	d_c (kpc)	$\log SM_c$ (kpc m ^{-20/3})	DM_c (pc cm ⁻³)	r_c (kpc)
B1741 – 312	-2.14	-1.00	8.50	1.40	89	0.01
1905 + 079	41.91	0.09	8.00	1.55	106	0.01
2008 + 33D	71.16	-0.09	2.35	0.35	27	0.01
2021 + 317	71.40	-3.10	2.35	-0.91	6	0.01
2023 + 336	73.10	-2.40	2.35	-0.20	14	0.01
2014 + 358	74.04	0.36	2.35	-0.09	16	0.01
2020 + 351	74.14	-1.01	2.35	0.68	39	0.01
2005 + 372	74.18	2.61	2.35	0.56	34	0.01
2048 + 313	74.60	-8.04	2.35	-0.09	16	0.01
2013 + 370	74.90	1.20	2.20	-0.45	11	0.01
2012 + 383	75.78	2.19	2.35	-0.05	17	0.01
2005 + 403	76.80	4.30	2.35	-0.00	18	0.01
2050 + 364	78.90	-5.10	2.35	-1.40	4	0.02
0241 + 622	135.70	2.40	2.20	-0.09	16	0.01

TABLE 6
CLUMP PARAMETERS FOR GALACTIC, NON-PULSAR LINES OF SIGHT

LOS	ℓ (deg)	b (deg)	d_c (kpc)	$\log SM_c$ (kpc m ^{-20/3})	DM_c (pc cm ⁻³)	r_c (kpc)
MonR2	-146.30	-12.60	0.41	-0.96	6	0.01
NGC6334N ^a	-8.80	0.65	1.67	3.61	142	0.01
OH353.298	-6.70	-1.54	8.40	6.35	886	0.05
OH355	-4.23	-1.75	8.40	6.46	886	0.05
OH357.849	-2.15	9.74	8.40	5.75	886	0.05
OH359.140	-0.86	1.14	8.40	7.00	886	0.05
OH359.540	-0.44	1.29	8.40	4.79	886	0.05
OH000.125 + 5.111	0.12	5.11	8.40	4.60	886	0.05
OH000.892 + 1.342	0.89	1.34	8.40	4.95	886	0.05
OH20.1 – 0.1	20.07	-0.09	4.00	3.56	177	0.01
OH35.2 – 1.7	35.20	-1.73	2.80	0.30	35	0.01
OH40.6 – 0.2	40.62	-0.14	2.20	3.75	53	0.00
W49N	43.16	0.01	8.50	1.69	124	0.02
OH43.80 – 0.13	43.78	-0.14	2.60	2.16	213	0.02
CygX – 3	79.85	0.70	2.35	1.69	124	0.02
W75S	81.80	0.64	2.40	1.69	124	0.02
CepA	109.87	2.10	0.60	0.16	21	0.02
NGC7538	111.54	0.77	3.40	-0.00	18	0.02
W3OH	133.95	1.06	2.20	3.80	354	0.02

^aThe clump toward NGC6334N also affects the strongly scattered extragalactic source, NGC6334B (see Paper II).

TABLE 7
 CLUMPS FOR PULSAR LINES OF SIGHT WITH $DM_c > 20 \text{ pc cm}^{-3}$ OR $\log SM_c > 0$

LOS	ℓ (deg)	b (deg)	d_c (kpc)	DM_c (pc cm^{-3})	$\log SM_c$ ($\text{kpc m}^{-20/3}$)	r_c (kpc)
0611 + 22	-171.21	2.40	0.65	23.2	...	0.01
GumI	-100.00	-1.00	0.50	110.5	...	0.14
GumII	-97.20	2.70	0.50	28.4	-0.59	0.03
VelaIras	-96.75	-9.00	0.25	269.4	1.54	0.04
J1019 - 5749	-76.20	-0.68	4.21	709.0	2.60	0.01
J1022 - 5813	-75.70	-0.83	4.21	354.5	2.60	0.01
J1031 - 6117	-73.12	-2.88	3.00	35.4	-0.70	0.02
J1056 - 6258	-69.71	-2.97	2.20	177.2	-0.13	0.02
1112 - 60	-68.56	-0.32	6.13	9.9	0.19	0.01
J1119 - 6127	-67.85	-0.54	2.30	35.4	-0.70	0.02
J1128 - 6219	-66.51	-0.97	2.30	35.4	0.60	0.02
1131 - 62	-65.79	-1.30	6.51	10.8	0.27	0.01
J1201 - 6306	-62.69	-0.79	2.00	78.0	-0.02	0.02
J1216 - 6223	-61.08	0.20	2.10	106.3	0.25	0.02
J1305 - 6256	-55.50	-0.12	8.00	354.5	2.60	0.01
J1324 - 6146	-53.10	0.85	8.00	354.5	2.60	0.01
1334 - 61	-51.63	0.30	6.50	13.5	0.46	0.01
1338 - 62	-51.27	-0.04	7.21	12.6	0.40	0.01
1430 - 6623	-47.35	-5.40	0.90	33.1	...	0.01
1508 - 57	-39.23	-0.11	3.00	88.6	...	0.01
1419 - 3920	-39.07	20.45	0.30	26.1	...	0.01
1627 - 47	-23.52	0.62	3.43	33.9	1.26	0.01
1630 - 44	-21.27	1.98	3.38	10.8	0.27	0.01
1641 - 45	-20.81	-0.20	3.40	53.2	0.25	0.02
1643 - 43	-18.89	0.97	3.34	10.8	0.27	0.01
1703 - 40	-14.28	-0.20	1.45	15.2	0.57	0.01
1718 - 36	-9.07	-0.00	1.50	72.0	...	0.01
1727 - 33	-5.87	0.09	1.48	21.4	0.86	0.01
1736 - 31	-2.90	-0.22	3.31	17.0	0.66	0.01
1746 - 30	-0.54	-1.24	2.00	77.3	...	0.01
1807 - 2715	3.84	-3.26	1.50	70.2	...	0.01
1758 - 23	6.81	-0.08	6.63	17.9	0.71	0.01
1815 - 14	16.41	0.61	4.83	11.7	0.34	0.01
1820 - 14	17.25	-0.18	3.50	301.3	...	0.01
1824 - 10	21.29	0.80	1.92	15.2	0.57	0.01
1836 - 1008	22.26	-1.42	2.00	47.1	...	0.01
1830 - 08	23.39	0.06	4.40	141.8	...	0.01
1832 - 06	25.09	0.55	2.06	36.5	1.32	0.01
1839 - 04	28.35	0.17	2.23	15.8	0.60	0.01
1849 + 00	33.30	0.10	7.40	354.5	3.60	0.02
1821 + 05	34.99	8.86	0.44	22.5	...	0.01
1900 + 01	35.73	-1.96	2.80	141.8	0.11	0.04
1859 + 07	40.57	1.06	3.50	35.4	-0.70	0.02
1907 + 10	44.83	0.99	0.60	34.6	...	0.01
1914 + 13	47.58	0.45	4.00	88.8	...	0.01
2044 + 46	85.43	2.11	2.00	177.2	2.00	0.01
2036 + 53	90.37	7.31	2.00	88.6	1.40	0.01

TABLE 8
VOID PARAMETERS

LOS (1)	ℓ (2)	b (3)	d_v (4)	n_{ev} (5)	F_v (6)	a_v (7)	b_v (8)	c_v (9)	θ_{vz} (10)
GumIedge	-81.50	-0.60	0.50	0.500	1.00	0.02	0.02	0.04	9.00
J1224 - 6407	-60.02	-1.42	1.90	0.002	0.10	0.50	0.05	0.10	30.00
J1453 - 6413	-44.27	-4.43	1.50	0.005	0.10	0.25	0.10	0.10	46.00
J1600 - 5044	-29.31	1.63	1.50	0.001	0.10	1.00	0.10	0.10	61.00
J1600 - 5044	-29.31	1.63	3.60	0.001	0.10	0.50	0.20	0.20	61.00
J1559 - 4438	-25.46	6.37	1.30	0.020	0.00	0.90	0.07	0.07	64.54
J1709 - 4428	-16.90	-2.68	1.50	0.010	0.10	0.40	0.10	0.10	73.00
1757 - 24	5.31	0.02	3.00	0.035	10.00	1.20	0.03	0.10	95.31
1759 - 2205	7.47	0.81	2.00	0.055	1.30	1.20	0.02	0.10	97.47
1821 - 24	7.80	-5.58	1.50	0.005	0.10	0.40	0.20	0.20	0.00
1534 + 12	19.85	48.34	0.35	0.004	0.00	0.20	0.20	0.30	-70.15
Interarm2 - 3	31.00	0.00	4.20	0.010	0.10	0.80	0.45	0.20	-25.00
1859 + 03	37.21	-0.64	6.00	0.100	1.00	0.90	0.02	0.04	127.21
Interarm3 - 4	45.00	0.00	2.00	0.024	0.10	0.80	0.30	0.20	-25.00
1915 + 13	48.26	0.62	3.00	0.024	20.00	0.20	0.20	0.20	-41.74
2334 + 61	114.28	0.23	2.50	0.005	0.10	0.50	0.10	0.10	24.00
0138 + 59	129.15	-2.10	1.50	0.017	0.10	0.70	0.10	0.10	39.00

The columns are (1) line of sight name; (2)-(3) Galactic coordinates in degrees; (4) void distance (kpc); (5) void electron density (cm^{-3}); (6) void fluctuation parameter; (7)-(9) ellipsoidal semi-axes (kpc); (10) rotation angle (degrees) of semi-major axis about the z axis, referenced to the x axis.

APPENDIX

A. LISM MODEL FORM

The local ISM is modeled with four components that augment the large scale Galactic features. These are the local hot bubble (LHB) in which the Sun sits, a low-density region (LDR) primarily in the first quadrant of the Galaxy, a local superbubble (LSB) region in the third quadrant, and the “Loop I” feature that includes the North Polar Spur (e.g. Berkhuijsen, Haslam, & Salter 1971; Spoelstra 1972)

We model the LDR and LSB as ellipsoids with one axis perpendicular to the plane of the Galaxy and the other making an angle θ with the x direction (i.e. $\ell = 90^\circ$). The semi-major axes are denoted a, b, c and the ellipsoid center is given by $\bar{x}, \bar{y}, \bar{z}$. The internal density n_e and fluctuation parameter F are also individual attributes for each region. Parameter values are given in Table 4.

For the LHB we use the work of Bhat et al.(1999), Sfeir et al.(1999), Vergely et al.(2001) and Maíz-Apellániz (2001) as a guide for defining its structure. Using contours of Na I absorption given by Sfeir et al.(1999), which delineate the absence of absorbing gas, and the electron density implied by X-ray observations (Snowden et al.1998), $n_e \sim 0.005 \text{ cm}^{-3}$, we define the LHB as follows. The LHB is a slanted, ellipsoidal cylinder with cross section in the $x - y$ plane described by the parameters a and b . The cylinder has total length $2c$ in the z direction and a mean z given by \bar{z} . For $z \geq 0$, the cylinder has constant cross section at constant z . For $z < 0$, a declines linearly, reaching zero at $z = \bar{z} - c$. the b parameter is constant for all z within the cylinder. Finally, the cylinder axis is slanted in the $y-z$ plane with angle $\tan \theta = dy/dz$. The internal density and fluctuation parameter are also parameters for the LHB. Parameter values are given in Table 4.

The Loop I component is modeled only for $z \geq 0$ as a hemisphere of radius r surrounded by a shell of thickness Δr . The hemispherical volume and shell have different internal densities and F values. Parameter values given in Table 4 are guided by those given by Heiles (1998) but result from fitting for the best values of the parameters.

All four LISM regions have internal electron densities that are less than those in the large-scale Galactic structures. Therefore, to ensure that densities are mutually exclusive (not additive) between different components, we combine components by assigning weight factors $w_{\text{hb}}, w_{\text{lsb}}, w_{\text{ldr}}$ and w_{loopI} to each region and, together, use them to define an overall LISM weight, w_{lism} . The weights are either 0 or 1. They are defined with the following hierarchy: LHB:LoopI:LSB:LDR:ISM, meaning that the LHB overrides all other components (LISM and large scale), Loop I overrides the LSB, the LSB overrides the LDR, and any LISM component overrides the large scale components. For the LDR and LSB, the weight is unity inside the e^{-1} contour of each ellipsoid while for the LHB, the weight is unity anywhere inside the cylinder. For Loop I, the weight is unity anywhere inside the hemispherical sphere or shell.

B. FORTRAN CODE

Our model is implemented in Fortran routines similar in functionality to those presented in TC93, but that represent a complete revision according to the new features presented in the main text. Copies of the source and input files are available over the Internet at <http://www.astro.cornell.edu/cordes/NE2001> and http://rsd-www.nrl.navy.mil/7213/lazio/ne_model/. The code is packaged as a tar file, `NE2001.tar`, that includes a makefile for compiling the code in a Unix/Linux environment.

The makefile can compile the code into either an interactive program (`make pgm`) or (static) library (`make lib`). The interactive program `NE2001` evaluates the model by returning the integrated measures (DM, SM, etc.) and/or distance given an input direction and DM or distance. The library `libNE2001.a` allows one to incorporate the Fortran routines into user-written programs. Compiling the library into a program would be in a manner similar to the following:

```
f77 -L/path/to/library/directory program.f -lNE2001.
```

Integrations are performed in the the subroutine `dmdsm`, which evaluates the model by making calls to subroutine `density_2001`. The call to `dmdsm` is of the form

```
call dmdsm(l,b,ndir,dm,dist,limit,sm,smtau,smtheta,smiso) .
```

Here the input data include Galactic longitude and latitude, `l` and `b` (in radians), and a flag `ndir` indicating whether distance is to be calculated from dispersion measure (`ndir` ≥ 0), or *vice-versa* (`ndir` < 0). In either case, `dm` and `dist` have units of pc cm^{-3} and kpc , respectively. A flag `limit` is set if `ndir` ≥ 0 and the model distance is a lower limit; this will occur, for example, if a large `dm` is specified at high Galactic latitude. The subroutine also returns four estimates of scattering measure, all having units $\text{kpc m}^{-20/3}$. The first, `sm`, conforms to the definition in Eq. (4) with uniform weighting along the line of sight. The next two estimates, `smtau` and `smtheta`, correspond to line-of-sight weightings appropriate for temporal and angular broadening of Galactic sources, respectively. Temporal broadening emphasizes scattering material midway between source and observer, while angular broadening favors material closest to the observer; see Eqs. (A14, B2) of Cordes, Weisberg, & Boriakoff (1985). The last estimate, `smiso`, uses the weighting appropriate for calculating the isoplanatic angle of scattering.

Integrations in `dmdsm` involve evaluations of the model at a given Galactic location (x, y, z) through a call to subroutine `density_2001`, where `x,y,z` are Galactocentric Cartesian coordinates, measured in kiloparsecs, with the axes parallel to $(l, b) = (90^\circ, 0^\circ)$, $(180^\circ, 0^\circ)$, and $(0^\circ, 90^\circ)$:

```

    call density_2001(x,y,z,
    . ne1,ne2,nea,negc,nelism,necN,nevN,
    . F1, F2, Fa, Fgc, Flism, FcN, FvN,
    . whicharm, wlism, wldr, wlhb, wlsb, wloopI,
    . hitclump, hitvoid, wvoid).

```

The routine returns values for the electron density in seven components (`ne1`, \dots , `nevN`), the corresponding F parameters (`F1`, \dots , `FvN`), followed by a series of integer-valued flags. The meanings of these flags are as follows:

1. `whicharm` = 0, \dots , 5 indicates which spiral arm contributes to the density, with numbering as in the text and where a zero value denotes an interarm region.
2. `wlism`, `wldr`, `wlhb`, `wlsb` and `wloopI` take on values of 0 or 1 as described in Appendix A.
3. `hitclump` denotes whether a clump has been intersected in the integration; if so, then `hitclump` denotes the clump number in the table of clumps; if not, `hitclump` = 0.
4. `hitvoid` works in the same fashion for voids; additionally, `wvoid` = 0,1 is used in evaluating the total density and indicates if a void has been hit (`wvoid` = 1).

The calling program, `NE2001`, is executed using command-line arguments that specify the Galactic longitude and latitude, an input DM or distance value, and a flag (`ndir`) that specifies whether a distance is calculated from DM (`ndir` \geq 0) or a DM calculated from an input distance (`ndir` < 0):

```

Usage: NE2001 l b DM/D ndir
        l (deg)
        b (deg)
        DM/D (pc cm-3 or kpc)
        ndir = 1 (DM->D)   -1 (D->DM)

```

Program `NE2001` uses output from `dmdsm` to calculate scattering and scintillation quantities by making suitable calls to a series of functions. Input distances, scattering measures, frequencies and velocities are in standard units (kpc, $\text{kpc m}^{-20/3}$, GHz, and km s^{-1}):

1. `tauiss(d,sm,nu)`: calculates the pulse broadening time, τ_d (ms). See Eq. 9.
2. `scintbw(d,sm,nu)`: calculates the scintillation bandwidth, $\Delta\nu_d$ (MHz). See Eq. 10.
3. `scintime(sm,nu,vperp)`: calculates the scintillation time, Δt_{ISS} (sec) (Cordes & Lazio 1991; Cordes & Rickett 1998).
4. `specbroad(sm,nu,vperp)`: calculates the spectral broadening, $\Delta\nu_b$ (Hz), that is proportional to the reciprocal of the scintillation time (Cordes & Lazio 1991).
5. `theta_xgal(sm,nu)`: calculates the angular broadening, θ_d (mas), appropriate for the scattering geometry for an extragalactic source. See Eq. 8.
6. `theta_gal(sm,nu)`: calculates the angular broadening, θ_d (mas), of a Galactic source. See Eq. 8.
7. `em(sm)`: calculates the emission measure, EM (pc cm^{-6}), associated with the scattering measure; note that the value calculated assumes a particular outer scale for a Kolmogorov wavenumber spectrum and represents a lower bound on EM (see Eq. 14).
8. `theta_iso(smiso,nu)`: calculates the isoplanatic angle, θ_{iso} (mas), the region on the sky over which scintillations are correlated.
9. `transition_frequency(sm,smtau,stheta,dintegrate)`: calculates the frequency of transition, ν_{trans} (GHz), between the weak and strong scattering regimes (Eq. 17).

Sample output for $\ell = 45^\circ$, $b = 5^\circ$, and $\text{DM} = 50 \text{ pc cm}^{-3}$ is:

```

#NE2001 input: 4 parameters
 45.0000      1      (deg)      GalacticLongitude
  5.0000      b      (deg)      GalacticLatitude
 50.0000      DM/D    (pc-cm-3_or_kpc)  Input_DM_or_Distance
  1           ndir    1:DM->D;-1:D->DM  Which?(DM_or_D)
#NE2001 output: 14 values
 2.6365      DIST    (kpc)      ModelDistance
 50.0000      DM      (pc-cm-3)      DispersionMeasure
  4.3578      DMz     (pc-cm-3)      DM_Zcomponent
0.3528E-03   SM      (kpc-m-20/3)    ScatteringMeasure
0.2367E-03   SMtau   (kpc-m-20/3)    SM_PulseBroadening
0.7719E-04   SMtheta (kpc-m-20/3)    SM_GalAngularBroadening
0.1307E-02   SMiso   (kpc-m-20/3)    SM_IsoplanaticAngle
0.1921E+00   EM      (pc-cm-6)      EmissionMeasure_from_SM
0.1293E-03   TAU     (ms)          PulseBroadening @1GHz
0.1428E+01   SBW     (MHz)         ScintBW @1GHz
0.4943E+03   SCINTIME (s)          ScintTime @1GHz @100 km/s
0.2420E+00   THETA_G (mas)         AngBroadeningGal @1GHz
0.1086E+01   THETA_X (mas)         AngBroadeningXgal @1GHz
 14.02      NU_T     (GHz)         TransitionFrequency

```

The Fortran program can be run using a perl script (also included in the tar file) which allows selection of an individual field for output:

```
run_NE2001.pl
```

Usage:

```

run_NE2001      1      b      DM/D      ndir      field
                 deg deg    pc-cm-3    1,-1    D etc
                 or kpc

```

Possible Fields (case insensitive):

```
Dist, DM, SM, EM, TAU, SBW, SCINTIME, THETA_G, THETA_X, NU_T, ALL
```